Sensorless Commutation Method for Low-Voltage BLDC Motors Based on Unfiltered Line Voltage

Shahin MAHDIYOUN RAD, Mohammad Reza AZIZIAN, Mohammad HEJRI

Faculty of Electrical Engineering, Sahand University of Technology,
New Sahand Town, Tabriz, Iran

s_mahdiuonrad@sut.ac.ir, azizian@sut.ac.ir, hejri@sut.ac.ir

DOI: 10.15598/aeee.v17i1.3021

Abstract. *This study presents a filterless and sensorless commutation method for low-voltage brushless DC motors. The proposed method utilizes controlled DC-link inverter instead of the Pulse-Width Modulation (PWM) scheme. Therefore, motor voltages and currents become free from the high-frequency noise of PWM switching, thereby decreasing motor losses. Consequently, the method does not require any Low-Pass Filter (LPF) and it does not involve speed-dependent phase delay caused by the LPF. However, current commutation deteriorates waveform of line voltages. Thus, specific functions are defined to compensate for the current commutation spikes and remove false zero-crossing points of line voltages. Furthermore, the use of unfiltered line voltages eliminates the requirement of any phase shifter. Hence, the main superiority of the proposed method over preceding sensorless commutation methods is the simultaneous elimination of the phase shifter and LPF, which makes the method simple and cost-effective. The simulation and experimental results show the effectiveness and validity of the method.*

Keywords

Brushless DC motor, current commutation, filterless, hysteresis, low-voltage, sensorless, rotor position detection.

1. Introduction

Brushless DC (BLDC) motor is widely used in the industry due to its high efficiency, low maintenance, light weight, and compact structure. The BLDC motors require the information of rotor position to perform current commutation in stator windings. However, the position sensors increase the complexity of system configuration as well as motor cost and size [1], [2] and [3]. Sensorless control methods have been introduced to cope with the abovementioned restrictions.

In [4] and [5] commutation points were extracted by detecting Zero-Crossing Points (ZCPs) of line voltage differences which were sampled during Pulse-Width Modulation (PWM) on time. Another method utilized a Z-source inverter to supply BLDC motor and sampled the voltage of the inactive phase in shoot-through vectors to detect its ZCPs [6]. The ZCPs of phase back Electro-Motive Force (EMF) advance inherently actual commutation points by 30°. Hence, a phase shifter is demanded to determine the commutation points correctly. The phase shifting process makes the sensorless commutation technique more sophisticated because it needs the high-cost Digital Signal Processor (DSP). Although the methods used in [4], [5] and [6] need no Low-Pass Filter (LPF), they require a particular PWM switching pattern to sample the motor voltages accurately.

Filtered line voltages that comprise the corresponding line back EMFs have been used in [7], [8] and [9] to estimate the commutation instants. The LPF, which is used to suppress high-frequency noise due to PWM switching of the inverter, causes speed-dependent phase delay that increases as rotor speed increases. The phase delay of the estimated position prevents the phase current from aligning with the rotor position. Therefore, it generates torque ripples that reduce the average torque and motor efficiency. Consequently, LPF limits the high-speed operation capability of BLDC motors [10]. In [9], phase delay caused by LPF was nearly compensated only at the rated speed of the motor by adjusting the hysteresis band of the comparators. Hence, this approach is inappropriate for variable speed drives. In [11] and [12], specific methods were presented based on shifting the ZCPs of heavily filtered line voltages by either $90 - \alpha$ or $150 - \alpha$ degrees. These methods were complicated and required

variable phase shifting. The technique presented in [13] also used line voltages. However, it was more complicated and needed two-step filtering and virtual neutral point.

In [14], [15] and [16], speed-independent functions are used to detect the commutation instants. The calculation of the speed-independent functions is complicated because they depend on the measured voltages, currents and the derivatives of the currents. Other studies have been dedicated to correction of the rotor position error. For example, commutation instants are adjusted by forcing the current integrals of the two half periods to be equal in 60 degrees conducting period [17]. It is reported that the effect of the estimated position error reflects on the current waveform. Hence, the current waveform is used as an index to compensate for the commutation error [18]. In the other study, a self-correction sensorless method is introduced based on the difference of the terminal voltage of the inactive phase between the beginning and the end of commutation interval [19].

The contribution of this study is an improvement of sensorless commutation of BLDC motors by the simultaneous elimination of the LPF and phase shifter. Commutation spikes of the unfiltered line voltages are investigated in detail in Sec. 2. Then, specific functions are presented in Sec. 3. to compensate for the false ZCPs caused by current commutation. The estimation error of the proposed and conventional methods are analyzed in Sec. 4. The simulation and experimental results are provided in Sec. 5. and Sec. 6. , respectively, to verify the effectiveness of the proposed approach. The results justify that the method can be easily implemented using simple circuits without any need for high-cost DSPs. Furthermore, the estimated commutation signals are phase-delay-free because no LPF is used anymore. Hence, the method can increase the operating range. Finally, conclusions are given in Sec. 7.

2. Spikes of Unfiltered Line Voltages

Usually, the PWM method is used to control BLDC motors. However, some studies have proved that supplying BLDC motor with a controlled DC-link inverter leads to high efficiency [20] and [21]. Figure 1 shows the equivalent circuit of a three-phase Y-connected BLDC motor which is fed by a full-bridge inverter, and a buck converter is used in front of the inverter to regulate the DC-link voltage by the duty cycle of switch S_7. Figure 2 shows the simulation waveforms of the phase current obtained from the PWM and controlled DC-link inverter schemes. It is evident that the

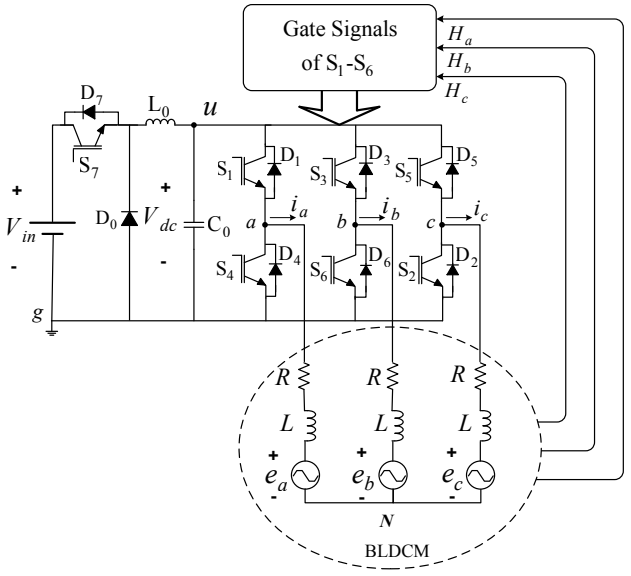

Fig. 1: The equivalent circuit of the Y-connected BLDC motor and its inverter topology based on the buck converter.

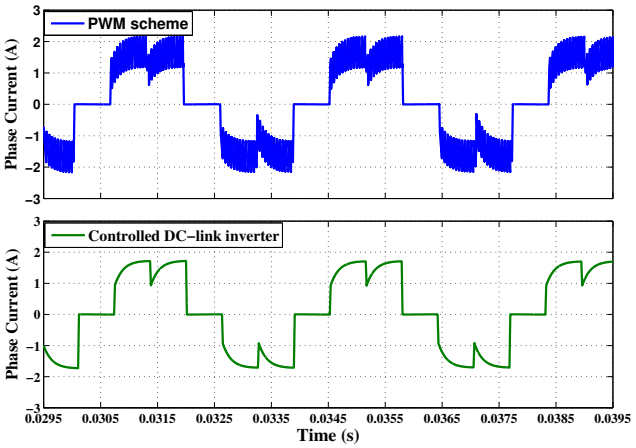

Fig. 2: Comparison of the phase currents obtained from the PWM scheme (top) and the controlled DC-link inverter scheme (bottom).

PWM method causes the large high-frequency ripple in the stator current which inevitably increases copper and iron losses. Furthermore, the controlled DC-link inverter could provide more stable performance for sensorless control of a BLDC motor than the PWM method [11], [12], [13], [20], [21], [22] and [23].

The voltage equations of the BLDC motor shown in Fig. 1 are given as:

$$\begin{bmatrix} V_{ag} \\ V_{bg} \\ V_{cg} \end{bmatrix} = R \begin{bmatrix} i_a \\ i_b \\ i_c \end{bmatrix} + L \frac{\mathrm{d}}{\mathrm{d}t} \begin{bmatrix} i_a \\ i_b \\ i_c \end{bmatrix} + \begin{bmatrix} e_a \\ e_b \\ e_c \end{bmatrix} + \begin{bmatrix} V_{Ng} \\ V_{Ng} \\ V_{Ng} \end{bmatrix}, \quad (1)$$

where V_{ag}, V_{bg}, and V_{cg} are the motor terminal voltages with respect to the DC-link ground g. The stator phase currents are indicated by i_a, i_b, and i_c. The stator resistance, stator inductance and motor neutral point voltage relative to the ground g are denoted by R, L,

and V_{Ng}, respectively. The maximum value of the back EMFs can be defined as:

$$E = K_e \omega_m, \tag{2}$$

where K_e and ω_m are the motor voltage constant and angular velocity, respectively. The trapezoidal back EMF voltages which are indicated by e_a, e_b and e_c can be expressed as:

$$\begin{aligned} e_a &= EF(\theta_e), \\ e_b &= EF\left(\theta_e - \frac{2\pi}{3}\right), \\ e_c &= EF\left(\theta_e + \frac{2\pi}{3}\right), \end{aligned} \tag{3}$$

where θ_e is electrical angular position of rotor and F stands for the trapezoidal function which can be given as:

$$F(\theta_e) = \begin{cases} \frac{6}{\pi}\theta_e & 0 \le \theta_e < \frac{\pi}{6}, \\ 1 & \frac{\pi}{6} \le \theta_e < \frac{5\pi}{6}, \\ 1 - \frac{6}{\pi}(\theta_e - \frac{5\pi}{6}) & \frac{5\pi}{6} \le \theta_e < \frac{7\pi}{6}, \\ -1 & \frac{7\pi}{6} \le \theta_e < \frac{11\pi}{6}, \\ -1 + \frac{6}{\pi}(\theta_e - \frac{11\pi}{6}) & \frac{11\pi}{6} \le \theta_e < 2\pi. \end{cases} \tag{4}$$

The inverter switches S_1–S_6 turn on and off only when they perform the current commutation. Therefore, the motor terminal voltages do not contain undesirable high-frequency switching noise, and thus, no LPF is employed anymore. Consequently, the proposed method does not involve the speed-dependent phase delay caused by LPF. Figure 3 shows the three line voltages along with the corresponding phase currents. When the BLDC motor operates with 120° conduction mode, there are six combinations of the stator excitation in a fundamental cycle. Under regular conduction interval, only two of the three phases are conducting at any time, and the other phase is unexcited. By performing current commutation every 60°, the commutation intervals will emerge. During the commutation intervals, the three phases conduct because the commutation needs a finite time due to the stator windings inductance. The six regular conduction intervals and six commutation intervals are indicated in Fig. 3 and Tab. 1.

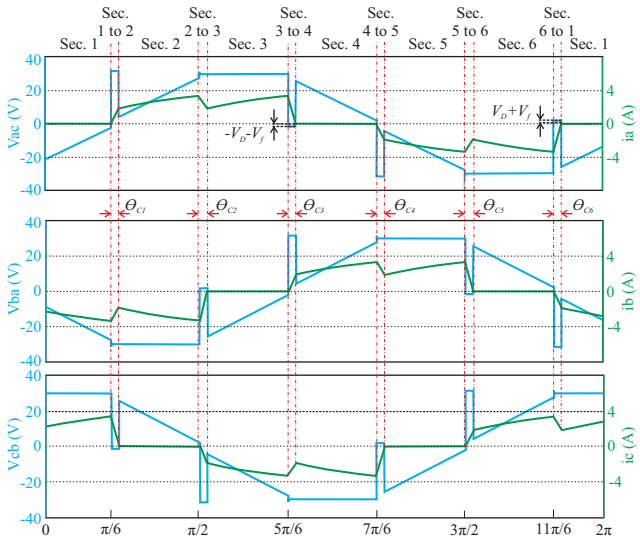

Fig. 3: Three unfiltered line voltages and corresponding phase currents.

Tab. 1: Six regular conduction and six commutation intervals.

Sec.	Interval	Conducting devices
1	$0 \le \theta_e < \pi/6$	S_5, S_6
1 to 2	$\pi/6 \le \theta_e < \pi/6 + \theta_{C1}$	S_1, S_6, D_2
2	$\pi/6 + \theta_{C1} \le \theta_e < \pi/2$	S_1, S_6
2 to 3	$\pi/2 \le \theta_e < \pi/2 + \theta_{C2}$	S_1, S_2, D_3
3	$\pi/2 + \theta_{C2} \le \theta_e < 5\pi/6$	S_1, S_2
3 to 4	$5\pi/6 \le \theta_e < 5\pi/6 + \theta_{C3}$	S_3, S_2, D_4
4	$5\pi/6 + \theta_{C3} \le \theta_e < 7\pi/6$	S_3, S_2
4 to 5	$7\pi/6 \le \theta_e < 7\pi/6 + \theta_{C4}$	S_3, S_4, D_5
5	$7\pi/6 + \theta_{C4} \le \theta_e < 3\pi/2$	S_3, S_4
5 to 6	$3\pi/2 \le \theta_e < 3\pi/2 + \theta_{C5}$	S_5, S_4, D_6
6	$3\pi/2 + \theta_{C5} \le \theta_e < 11\pi/6$	S_5, S_4
6 to 1	$11\pi/6 \le \theta_e < 11\pi/6 + \theta_{C6}$	S_5, S_6, D_1

It can be seen from Fig. 3 that the current commutation causes four voltage spikes in each line voltage waveform; while only two of them cross the horizontal axis and cause zero-crossing errors. Let us calculate the amplitude of line voltage V_{ac} during the critical commutation spikes which make false ZCPs in the line voltage waveforms (see Fig. 3 and highlighted rows in Tab. 1). Consider Sec. 3 in which switches S_1 and S_2 are conducting, and commutation instant comes and makes switch S_1 turn off and switch S_3 turn on. This switching leads to transferring current from a–phase to b–phase. As mentioned before, due to the inductance of stator windings, the current of a–phase does not decrease to zero immediately. Hence, diode D_4 conducts until i_a becomes zero. This current commutation causes a spike in the waveform of line voltage V_{ac} which is indicated as **Sec. 3 to 4** in Fig. 3. The equivalent circuit during this commutation interval is shown in Fig. 4(a). By applying KVL to the path traced from a to c, the amplitude of line voltage V_{ac} is obtained as $-V_D - V_f$, where V_D and V_f denote diode and transistor forward voltage drops, respectively. Now, let us consider the negative half cycle of line voltage V_{ac}. Consider Sec. 6 in which switches S_4 and S_5 are conducting, and commutation instant reaches and makes switch S_4 turn off and switch S_6 turn on. The current of a–phase does not decrease to zero instantly, so it makes diode D_1 conduct until i_a becomes zero. This current commutation generates a spike in the waveform of line

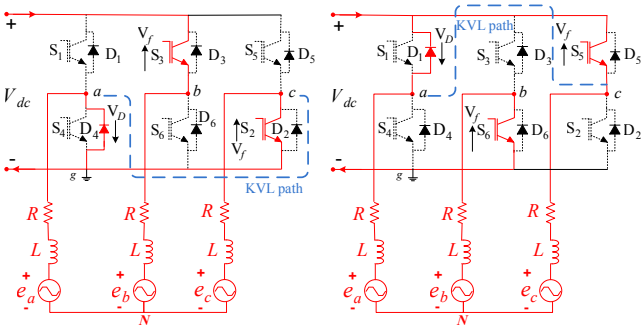

(a) Sec. 3 to 4. (b) Sec. 6 to 1.

Fig. 4: Equivalent circuit of the motor and its inverter during commutation interval.

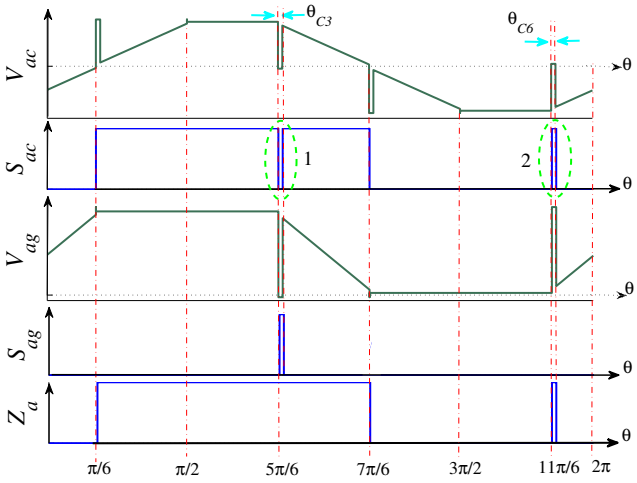

Fig. 5: Function S_{ag} used to compensate for the first spike of V_{ac} and the resultant signal Z_a.

voltage V_{ac} which is indicated as **Sec. 6 to 1** in Fig. 3. The equivalent circuit of the motor and inverter during this commutation interval is shown in Fig. 4(b). By applying KVL to the path shown in Fig. 4(b), the amplitude of line voltage V_{ac} is obtained as $V_D + V_f$. It can be concluded that the absolute value of the line voltages during the commutation intervals is the sum of the forward voltage drops on the diode and transistor $V_D + V_f$. In the case of a low-voltage BLDC motor, $V_D + V_f$ is large enough to be detected compared to the peak value of line voltages. That is not the case, however, if a high-voltage BLDC motor is considered. Hence, in this study, we focus on low-voltage BLDC motors.

3. Compensation for Commutation Spikes

We define a function for line voltage V_{ac} as:

$$S_{ac} = \text{Sign}(V_{ag} - V_{cg}), \tag{5}$$

where Sign operator is defined as:

$$\text{Sign}(x) = \begin{cases} 0 & x \leq 0, \\ 1 & x > 0. \end{cases} \tag{6}$$

Figure 5 shows line voltage V_{ac} and its function. Elliptical contours indicate the two commutation spikes in the function of the line voltage. The voltage of a–phase relative to the ground (V_{ag}) is also illustrated in Fig. 5.

V_{ag} can be expressed as:

$$V_{ag} = \begin{cases} \frac{V_{dc}}{2} + E\frac{6}{\pi}\theta_e & 0 \leq \theta_e < \frac{\pi}{6}, \\ V_{dc} - V_f & \frac{\pi}{6} \leq \theta_e < \frac{5\pi}{6}, \\ -V_D & \frac{5\pi}{6} \leq \theta_e < \frac{5\pi}{6} + \theta_{C3}, \\ \frac{V_{dc}}{2} + 6E(1 - \frac{\theta_e}{\pi}) & \frac{5\pi}{6} + \theta_{C3} \leq \theta_e < \frac{7\pi}{6}, \\ V_f & \frac{7\pi}{6} \leq \theta_e < \frac{11\pi}{6}, \\ V_{dc} + V_D & \frac{11\pi}{6} \leq \theta_e < \frac{11\pi}{6} + \theta_{C6}. \end{cases} \tag{7}$$

The maximum value of back EMFs, E, is always less than $V_{dc}/2$. Hence, according to Eq. (7), V_{ag} indicates a positive value except within the interval from $5\pi/6$ to $5\pi/6 + \theta_{C3}$ in which D_4 is conducting and the amplitude of V_{ag} is $-V_D$. This interval coincides with the first spike of voltage V_{ac}. Hence, we define a Sign function for V_{ag} as:

$$S_{ag} = \bar{\text{Sign}}(V_{ag}). \tag{8}$$

The above function can compensate for the first spike of voltage V_{ac} by utilizing the logical equation:

$$Z_a = S_{ac} + S_{ag}, \tag{9}$$

where $+$ stands for OR operator. Figure 5 depicts the function S_{ag} and the resultant signal (Z_a). As can be seen, the function S_{ag} compensates for the first spike of the function S_{ac}. However, the effect of the second spike still deteriorates the resultant signal Z_a. By detailed investigation on the waveform of voltage V_{ag}, another fact is discovered that the amplitude of V_{ag} is greater than the DC-link voltage only in the interval from $11\pi/6$ to $11\pi/6 + \theta_{C6}$ which coincides with the second spike of the line voltage V_{ac}. In this interval,

diode D_1 is conducting and the value of V_{ag} is $V_{dc}+V_D$. Accordingly, we define another function as:

$$S_{ua} = \text{Sign}(V_{ug} - V_{ag}), \tag{10}$$

where V_{ug} is the voltage of the positive rail of DC-link to the ground. Figure 6 shows voltage V_{ua}, its function S_{ua}, and the signal Z_a obtained from Eq. (9). As evident from Fig. 6, the function S_{ua} can be used to compensate for the second spike of voltage V_{ac} by using the logical equation:

$$C_a = Z_a \bullet S_{ua} = (S_{ac} + S_{ag}) \bullet S_{ua}, \tag{11}$$

where $\bullet$ stands for AND operator. The resultant spike-free commutation signal C_a is illustrated in Fig. 6. The same process is applied to the other two unfiltered line voltages, namely, V_{ba} and V_{cb}. Accordingly, the appropriate functions which are required to compensate for the spikes caused by current commutation are defined as:

$$\begin{aligned}
S_{ba} &= \text{Sign}(V_{bg} - V_{ag}),\\
S_{bg} &= \bar{\text{Sign}}(V_{bg}),\\
S_{ub} &= \text{Sign}(V_{ug} - V_{bg}),\\
S_{cb} &= \text{Sign}(V_{cg} - V_{bg}),\\
S_{cg} &= \bar{\text{Sign}}(V_{cg}),\\
S_{uc} &= \text{Sign}(V_{ug} - V_{cg}).
\end{aligned} \tag{12}$$

The commutation signals of b– and c–phases can be extracted as:

$$\begin{aligned}
C_b &= (S_{ba} + S_{bg}) \bullet S_{ub},\\
C_c &= (S_{cb} + S_{cg}) \bullet S_{uc}.
\end{aligned} \tag{13}$$

The proposed logical equations for generating six gating signals of the inverter from three estimated commutation signals can be derived as:

$$\begin{aligned}
G_{aH} &= C_a \bullet \bar{C}_b, \quad G_{aL} = C_b \bullet \bar{C}_a,\\
G_{bH} &= C_b \bullet \bar{C}_c, \quad G_{bL} = C_c \bullet \bar{C}_b,\\
G_{cH} &= C_c \bullet \bar{C}_a, \quad G_{cL} = C_a \bullet \bar{C}_c.
\end{aligned} \tag{14}$$

where subscripts kH and kL $(k = a, b, c)$ stand for high-side and low-side power devices of the inverter.

4. Error Analysis

4.1. Voltage Drop on Stator Resistance

The proposed method uses the line voltages to detect the ZCPs of the line back EMFs indirectly. Although the line voltages comprise the relevant line back EMFs, estimation error is inevitable because of voltage drop on the stator winding resistance. Assume that a– and c–phases are conducting and b–phase is unexcited. The

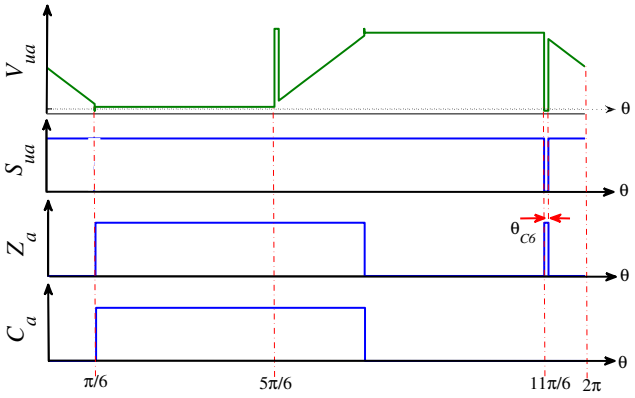

Fig. 6: Function S_{ua} used to compensate for the second spike of V_{ac} and the extracted commutation signal C_a.

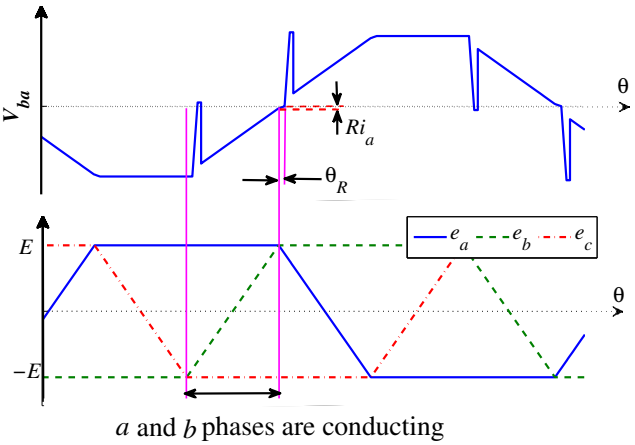

Fig. 7: Phase delay due to voltage drop on stator resistance.

indicated area in Fig. 7 corresponds to the mentioned interval. As can be seen, the back EMF of b–phase increases until it reaches its maximum value. The ideal commutation point for transferring current from a–phase to b–phase is the instant in which e_b equals e_a. However, in practice, the ZCPs of the line voltages are used to estimate the commutation points. Assume that the phase inductance is small enough to be neglected. In this case, when $e_{ba} = 0$ the line voltage can be expressed as:

$$V_{ba} = -Ri_a, \tag{15}$$

which means that the ZCPs of the line voltages do not coincide with those of the line back EMFs. Hence, the inverter switches keep their states unchanged until the line voltage crosses zero. The line voltage can be expressed as:

$$V_{ba} = e_b - e_a - Ri_a. \tag{16}$$

Substitution of the back EMFs defined in Eq. (3) in Eq. (16) gives:

$$V_{ba} = E - E(1 - \frac{6}{\pi}\theta_e) - Ri_a = \frac{6}{\pi}\theta_e E - Ri_a. \tag{17}$$

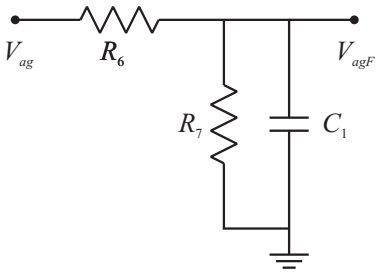

Fig. 8: The LPF used in the conventional sensorless methods.

The commutation point is detected when V_{ba} reaches zero. Hence, the rotor position estimation error can be derived as:

$$\theta_R = \left(\frac{Ri_a}{E}\right)\frac{\pi}{6}, \tag{18}$$

where the peak value of the back EMF can be extracted as:

$$E = \frac{V_{dc} - 2V_f - 2Ri_a}{2}. \tag{19}$$

By substituting Eq. (19) into Eq. (18), the phase delay caused by the voltage drop on stator resistance can be expressed as:

$$\theta_R = \left(\frac{Ri_a}{V_{dc} - 2V_f - 2Ri_a}\right)\frac{\pi}{3}. \tag{20}$$

4.2. Phase Delay Due to LPF

The LPF is used in the conventional sensorless commutation methods based on filtered voltages of the motor. Figure 8 shows a common LPF which is utilized in the conventional sensorless methods. The transfer function of the LPF can be given as:

$$\frac{V_{agF}}{V_{ag}} = \frac{R_7}{R_6 + R_7 + R_6R_7C_1s}. \tag{21}$$

The value of the phase delay caused by the LPF can be expressed as:

$$\theta_F = \arctan\left(\frac{R_6R_7C_1\omega_e}{R_6 + R_7}\right) = \arctan\left(\frac{\omega_e}{\omega_c}\right), \tag{22}$$

where ω_e is the electrical angular velocity of the rotor and ω_c is the cutoff frequency of the LPF. It can be concluded from Eq. (22) that the LPF causes the speed-dependent phase delay in the estimation of rotor position.

5. Simulation Results

Table 2 lists the specifications of the BLDC motor which is used to run the simulations in MATLAB/Simulink. To verify the effectiveness of the proposed method, we have compared its results with those

Tab. 2: Specifications of EC-22-167129 Maxon BLDC motor.

Parameters	Value
Rated power	50 [W]
Speed constant	702 [r·min^{-1}·V^{-1}]
Torque constant	13.6×10^{-3} [N·m·A^{-1}]
Pole pairs	1
Rated voltage	32 [V]
Rotor inertia	4.2×10^{-7} [kg.m^2]
Stator resistance	0.4985 [Ω]
Stator inductance	0.0735 [mH]
Rated speed	20200 [r·min^{-1}]
Voltage constant	13.6×10^{-3} [V·(rad·s^{-1})$^{-1}$]

of the conventional method based on ZCPs detection of the filtered line voltages. We choose the cutoff frequency of 2 kHz for the LPF of the conventional method to make a compromise between the phase delay of the LPF and its capability to remove the high-frequency noise.

The line voltage, phase current, electromagnetic torque, rotor speed, ideal Hall signal obtained by the Hall-effect position sensors placed within the motor, and the estimated commutation signals obtained from the proposed and conventional methods are shown in Fig. 9 and Fig. 10, respectively. These simulation results are given under the intermediate load at a speed of 15000 r·min^{-1}. By comparing the electromagnetic torque and phase current waveforms, it can be deduced that the proposed method causes less distortion in the current and torque waveforms than the conventional technique. The phase current and torque of the con-

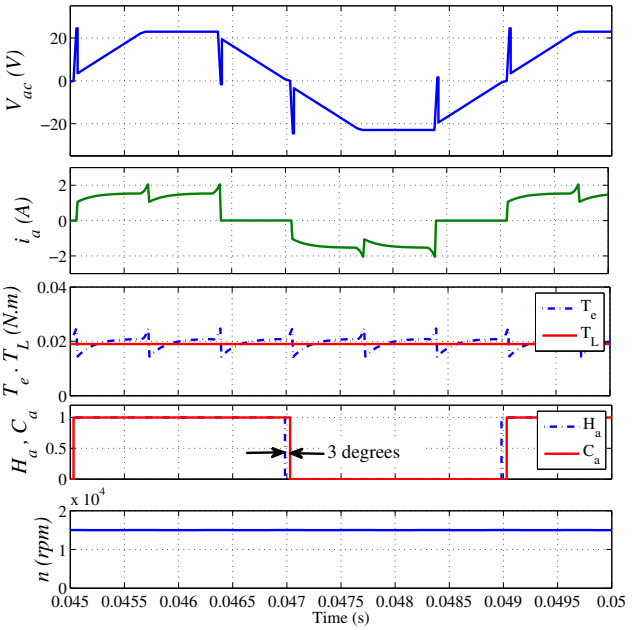

Fig. 9: Simulated waveforms of the proposed method under intermediate load at speed of 15000 r·min^{-1} (from top to bottom): unfiltered line voltage, phase current, electromagnetic torque, ideal and estimated commutation signals, and rotor speed.

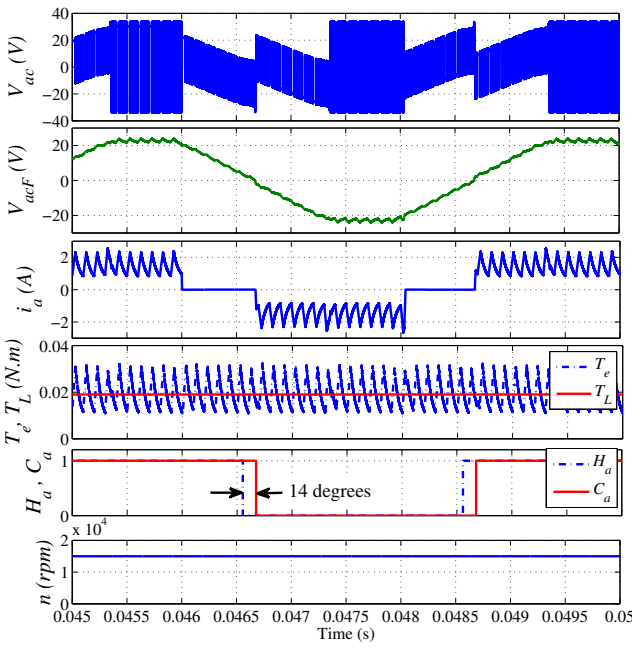

Fig. 10: Simulated waveforms of the conventional method under intermediate load at speed of 15000 r·min^{-1} (from top to bottom): unfiltered line voltage, filtered line voltage, phase current, electromagnetic torque, ideal and estimated commutation signals, and rotor speed.

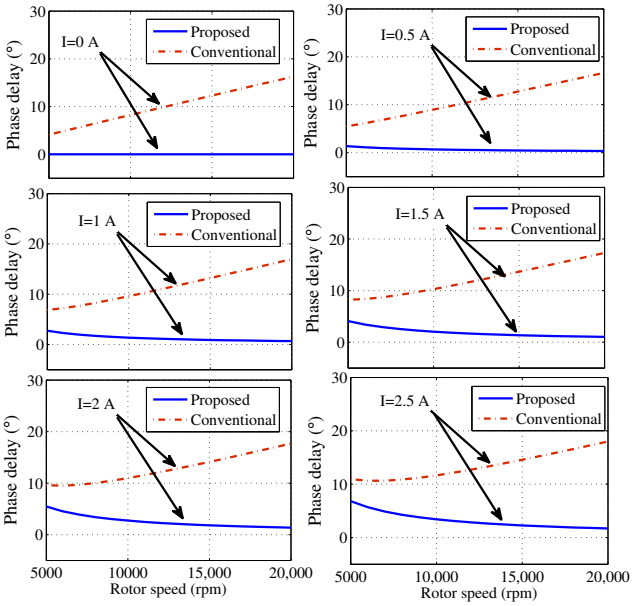

Fig. 11: Comparison of the simulated phase-delay vs. rotor speed under various load conditions for the proposed and conventional methods.

ventional method involve large high-frequency ripples that cause a decrease in the motor efficiency. Furthermore, the estimated commutation signal obtained from the proposed method has a good match with the ideal Hall signal. For the proposed method the commutation angle error is about 3°, whereas it is significant and about 14° for the conventional method. The small difference between the ideal Hall signal and the estimated commutation signal obtained from the proposed method is due to the phase delay resulting from voltage drop on the stator resistance. In the case of the conventional technique, the error caused by the voltage drop on the stator resistance superimposes to the error resulting from the LPF.

We repeated the simulation under different rotor speeds and phase currents to compare the position estimation error of the proposed method with that of the conventional method. Figure 11 shows the simulated performance of the proposed and conventional methods at different speeds, from 5000 to 20000 r·min^{-1}, under various load conditions with phase current of 0, 0.5, 1, 1.5, 2, and 2.5 A. In all the conditions, the commutation angle error of the proposed method is smaller than that of the conventional method, as expected. Due to the phase delay caused by LPF, the commutation angle error for the conventional method is significant at high speeds. Hence, as mentioned before, the conventional method is not suitable for a wide range of speed. On the contrary, increasing or decreasing the rotor speed does not affect the performance of the proposed method significantly.

Let us analyze the effect of the estimation error of the rotor position on smooth torque generating capability of the BLDC motor. Assume that the current commutation from c–phase to a–phase is performed with a phase delay of θ_d from the ideal commutation point. In this case, by ignoring the commutation interval, the 60° period of Sec. 2 can be expressed as:

$$\frac{\pi}{6} + \theta_d < \theta_e \leq \frac{\pi}{2} + \theta_d. \tag{23}$$

During this interval, the phase currents can be expressed as:

$$i_a = I, \qquad i_b = -I, \qquad i_c = 0. \tag{24}$$

The electromagnetic torque produced by the BLDC motor is given by:

$$T_e = \frac{K_t}{2}\left(F(\theta_e)i_a + F\left(\theta_e - \frac{2\pi}{3}\right)i_b + \right. \\ \left. + F\left(\theta_e + \frac{2\pi}{3}\right)i_c\right), \tag{25}$$

where K_t is the torque constant of the motor. Substituting Eq. (24) and Eq. (4) into Eq. (25) gives:

$$T_e = \frac{K_t}{2} I \begin{cases} 2 & \frac{\pi}{6} + \theta_d < \theta_e \leq \frac{\pi}{2}, \\ 5 - \frac{6\theta_e}{\pi} & \frac{\pi}{2} < \theta_e \leq \frac{\pi}{2} + \theta_d. \end{cases} \tag{26}$$

Accordingly, the average electromagnetic torque of the motor can be expressed as:

$$T_{av} = \frac{3}{\pi}\frac{K_t}{2} I \left(\int_{\frac{\pi}{6}+\theta_d}^{\frac{\pi}{2}} 2\mathrm{d}\theta_e + \int_{\frac{\pi}{2}}^{\frac{\pi}{2}+\theta_d} \left(5 - \frac{6\theta_e}{\pi}\right) \mathrm{d}\theta_e \right)$$
$$= \frac{K_t}{2} I \left(2 - \left(\frac{3}{\pi}\theta_d\right)^2\right). \quad (27)$$

Figure 12 shows the electromagnetic torque of the BLDC motor when current commutation happens with a phase delay. This figure and Eq. (27) justify that the maximum torque occurs at $\theta_d = 0$ with $K_t I$. Clearly, the larger the rotor position estimation error, the larger the torque ripple. In other words, the average electromagnetic torque produced by the BLDC motor decreases with increasing the estimation error of the rotor position. Therefore, the proposed method improves the efficiency and performance of the position sensorless drive of the BLDC motor by decreasing the estimation error of the rotor position.

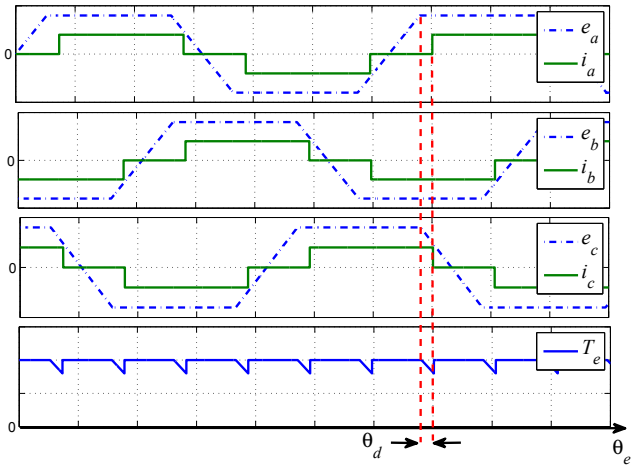

Fig. 12: Effect of the current commutation delay on torque generating capability of BLDC motor.

Figure 13 shows the waveforms of V_{ac}, i_a, rotor speed, load torque, and electromagnetic torque with sudden load change. The load torque has been increased suddenly from 0.01 to 0.037 N·m and after a while decreased from 0.037 to 0.01 N·m. As can be seen, the proposed sensorless commutation method has the effective performance for a sudden load change. Figure 14 shows the waveforms of V_{ac}, i_a, and rotor speed with speed change. The speed command has been increased from 4000 to 15000 r·min^{-1}. As can be seen, the proposed sensorless commutation method has the effective performance, and the motor continues to run during the transient conditions.

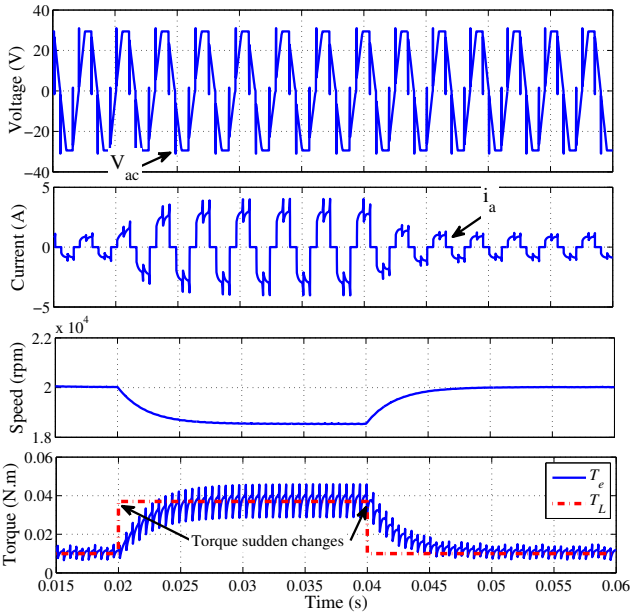

Fig. 13: Simulated waveforms of V_{ac}, i_a, rotor speed, load torque, and electromagnetic torque during load sudden change.

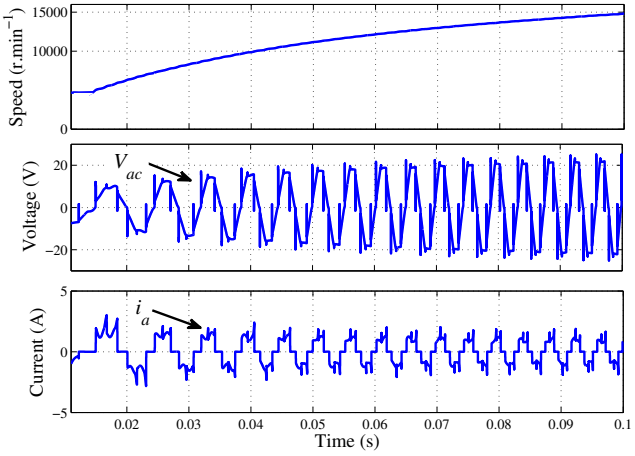

Fig. 14: Simulated waveforms of the rotor speed, V_{ac}, and i_a with speed change.

6. Experimental Results

Figure 15 shows the designed circuit to generate the proposed functions S_{ac}, S_{ag}, and S_{ua} that are required to extract the sensorless commutation signal of a–phase, namely, C_a. We have implemented the proposed method using low-cost LM339 comparators, CD4071 OR gate, CD4081 AND gate, and CD4069 logic inverter. Table 3 lists the prototype's parts and their cost from Amazon.com during November 2018. The Total cost of the proposed method is less than $10.

In circuits 1 and 2 shown in Fig. 15, voltages V_{ag}, V_{ug}, and V_{cg} are fed to the subtracters to generate voltage V_{ac} and V_{ua}. In the next step, these voltages are

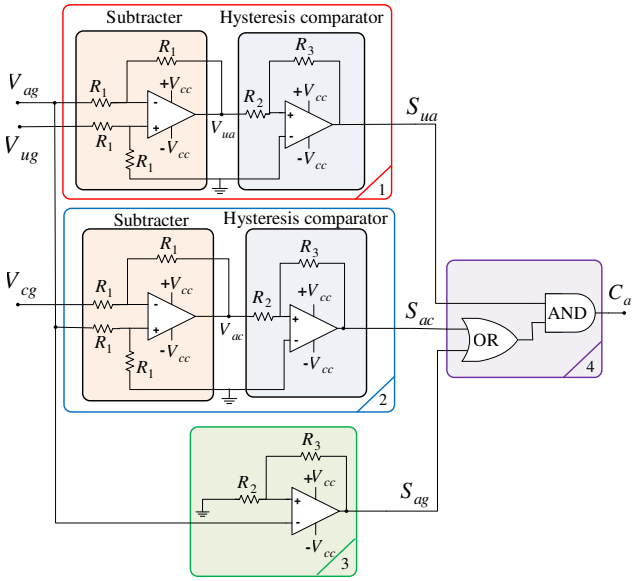

Fig. 15: The designed circuit for generating the estimated commutation signal for a–phase.

Tab. 3: Cost of the proposed method.

Component	Number	Price/Item
LM339	5	\$0.7
CD4071	1	\$1.3
CD4081	3	\$1.4
CD4069	1	\$0.8
Total	10	\$9.8

applied to the hysteresis comparators to create functions S_{ac}, and S_{ua}. The comparators with a hysteresis band yields noise-free and cleaner zero-crossing signals. A small hysteresis of 100 mV is integrated into the comparators to prevent the noise within the hysteresis band from crossing the threshold and producing false ZCPs. Therefore, additional noise immunity and stability can be obtained, and the performance of the sign generator circuit could be improved. In circuit 3, voltage V_{ag} is applied to a hysteresis comparator to implement Eq. (8) and generate sign function S_{ag}. Circuit 4 applies Eq. (11) to the sign functions and generates the commutation signal for a–phase. The similar approach is adopted to derive the other two commutation signals. Figure 16(a) shows the single-sided printed circuit boards (PCBs) that are designed and developed based on Eq. (8), Eq. (9), Eq. (10), Eq. (11), Eq. (12), Eq. (13) and Eq. (14). The overall view of the assembled experimental setup is illustrated in Fig. 16(b). The setup includes a Maxon BLDC motor with the specifications listed in Tab. 2, a DC generator (used as the load), a digital oscilloscope, the designed circuits (for the proposed sensorless operation), and a three-leg inverter. Moreover, a Lutron DT-2236C digital tachometer is used to measure the rotor speed. The phase currents are measured through the small resistors connected in series with the motor phases. Simple

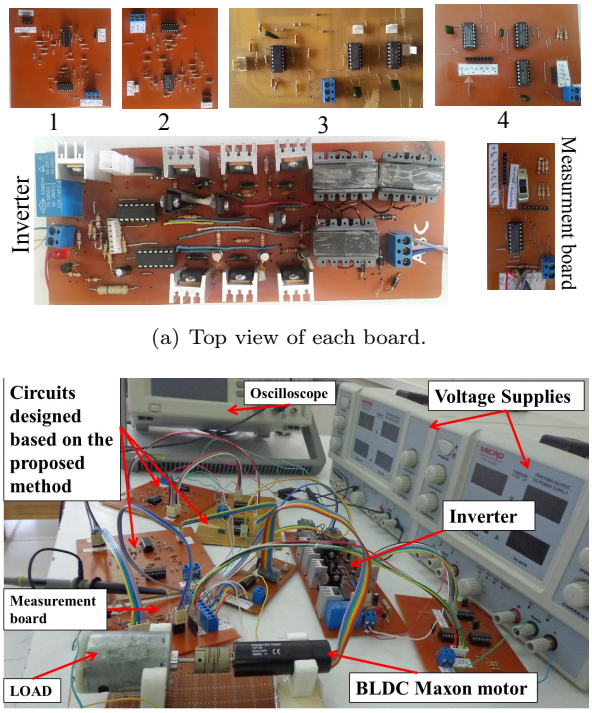

(a) Top view of each board.

(b) Assembled setup.

Fig. 16: Developed experimental setup.

resistive voltage dividers are used to measure the terminal voltages of the motor.

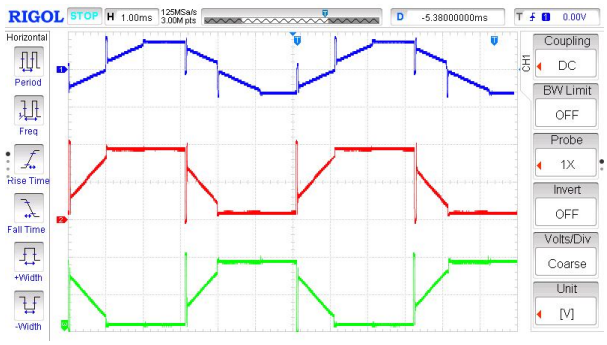

(a) V_{ac} (20 V/div), V_{ag} (10 V/div), and V_{ua} (10 V/div).

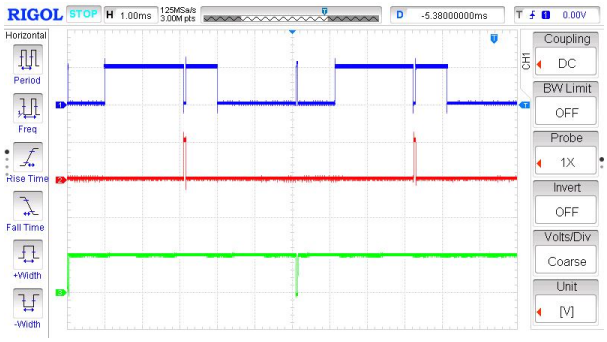

(b) S_{ac}, S_{ag}, and S_{ua} (5 V/div).

Fig. 17: Experimental waveforms.

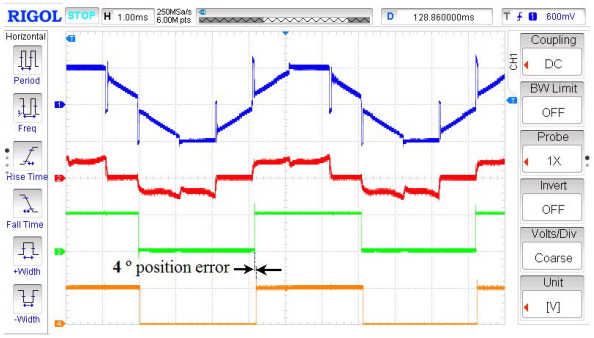

Fig. 18: Experimental signals obtained from the proposed method at speed of 10000 r·min^{-1} (from top to bottom): line voltage (20 V/div), phase current (2 A/div), ideal Hall signal (5 V/div), and the extracted commutation signal (5 V/div).

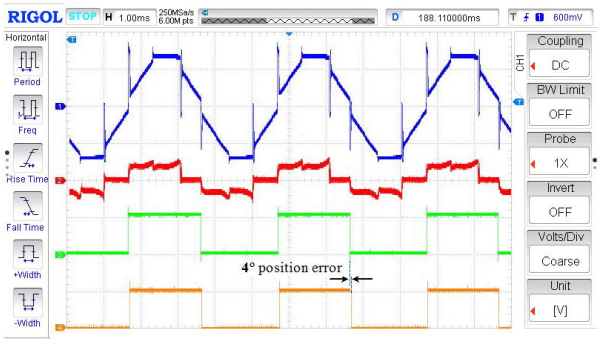

Fig. 19: Experimental signals obtained from the proposed method at speed of 15000 r·min^{-1} (from top to bottom): line voltage (20 V/div), phase current (2 A/div), ideal Hall signal (5 V/div), and the extracted commutation signal (5 V/div).

The experimental waveforms of V_{ac}, V_{ag}, and V_{ua} along with their sign functions S_{ac}, S_{ag}, and S_{ua} are illustrated in Fig. 17. They justify the capability of the designed circuits to generate the compensator functions accurately. The experimental waveforms of the line voltage, phase current, ideal Hall signal and the estimated commutation signal at speeds of 10000 and 15000 r·min^{-1} are shown in Fig. 18 and Fig. 19, respectively. The position error resulted by the proposed method is negligible and about 4°. The estimated position error of the proposed method is not significantly affected by the rotor speed, as expected. Furthermore, the phase current has the acceptable rectangular waveform.

7. Conclusion

This study presents a new sensorless commutation method for BLDC motors. The proposed method uses unfiltered line voltages. Thus, neither LPF nor phase shifter is required. The specific functions are introduced to compensate for the commutation spikes. The commutation signals are derived by the proposed logical equations. The simulation and experimental results prove the validity of the proposed method. Compared with the conventional sensorless methods, the proposed method has advantages as follow:

- Wide speed range due to the elimination of the LPFs.
- Simple and easy-to-implement due to the absence of the phase shifter.
- Cost-effective: The proposed method can be easily implemented using simple comparators without any need for high-cost DSPs.
- Precise commutation: position error and torque ripple are reduced due to the elimination of the LPFs.
- Insensitive to operating speed and load conditions.

References

[1] XU, Y., Y. WEI, B. WANG and J. ZOU. A Novel Inverter Topology for Brushless DC Motor Drive to Shorten Commutation Time. *IEEE Transactions on Industrial Electronics*. 2016, vol. 63, iss. 2, pp. 796–807. ISSN 0278-0046. DOI: 10.1109/TIE.2015.2480759.

[2] LEE, A. C., C.-J. FAN and G.-H. CHEN. Current Integral Method for Fine Commutation Tuning of Sensorless Brushless DC Motor. *IEEE Transactions on Power Electronics*. 2017, vol. 32, iss. 12, pp. 9249–9266. ISSN 0885-8993. DOI: 10.1109/TPEL.2017.2652847.

[3] LEE, A.-C., S. WANG and C. J. FAN. A Current Index Approach to Compensate Commutation Phase Error for Sensorless Brushless DC Motors With Nonideal Back EMF. *IEEE Transactions on Power Electronics*. 2016, vol. 31, iss. 6, pp. 4389–4399. ISSN 0885-8993. DOI: 10.1109/TPEL.2015.2468081.

[4] DAMODHARAN, P. and K. VASUDEVAN. Sensorless Brushless DC Motor Drive Based on the Zero-Crossing Detection of Back Electromotive Force (EMF) From the Line Voltage Difference. *IEEE Transactions on Energy Conversion*. 2010, vol. 25, iss. 3, pp. 661–668. ISSN 0885-8969. DOI: 10.1109/TEC.2010.2041781.

[5] ZHANG, X. Z. and Y. N. WANG. A Novel Position-Sensorless Control Method for Brushless DC Motors. *Energy Conversion and Management*. 2011, vol. 52, iss. 3, pp. 1669–1676. ISSN 0196-8904. DOI: 10.1016/j.enconman.2010.10.030.

[6] CHANGLIANG, X. and L. XIMIN. Z-Source Inverter-Based Approach to the Zero-Crossing Point Detection of Back EMF for Sensorless Brushless DC Motor. *IEEE Transactions on Power Electronics*. 2015, vol. 30, iss. 3, pp. 1488–1498. ISSN 0885-8993. DOI: 10.1109/TPEL.2014.2317708.

[7] KIM, T. Y. and J. LYOU. Commutation Instant Detector for Sensorless Drive of BLDC Motor. *Electronics Letters*. 2011, vol. 47, iss. 23, pp. 1269–1270. ISSN 0013-5194. DOI: 10.1049/el.2011.1956.

[8] MAHDIUON-RAD, S., M. R. AZIZIAN and S. SOLEYMANPOUR. Modeling, Simulation and Implementation of a Sensorless Commutation Method for Brushless DC Motors Without Phase Shifter. In: *Power Electronics, Drives Systems and Technologies Conference (PEDSTC)*. Tehran: IEEE, 2015, pp. 228–233. DOI: 10.1109/PEDSTC.2015.7093279.

[9] TAE-WON, C., T. QUANG-VINH, L. HONG-HEE and K. HEUNG-GEUN. Sensorless Control of BLDC Motor Drive for an Automotive Fuel Pump Using a Hysteresis Comparator. *IEEE Transactions on Power Electronics*. 2014, vol. 29, iss. 3, pp. 1382–1391. ISSN 0885-8993. DOI: 10.1109/TPEL.2013.2261554.

[10] XIA, C., Y. XIAO, W. CHEN and T. SHI. Torque Ripple Reduction in Brushless DC Drives Based on Reference Current Optimization Using Integral Variable Structure Control. *IEEE Transactions on Industrial Electronics*. 2014, vol. 61, iss. 2, pp. 738–752. ISSN 0278-0046. DOI: 10.1109/TIE.2013.2254093.

[11] LIU, G., C. CUI, K. WANG, B. HAN and S. ZHENG. Sensorless Control for High-Speed Brushless DC Motor Based on the Line-to-Line Back EMF. *IEEE Transactions on Power Electronics*. 2016, vol. 31, iss. 7, pp. 4669–4683. ISSN 0885-8993. DOI: 10.1109/TPEL.2014.2328655.

[12] CHENJUN, C., L. GANG, W. KUN and S. XINDA. Sensorless Drive for High-Speed Brushless DC Motor Based on the Virtual Neutral Voltage. *IEEE Transactions on Power Electronics*. 2015, vol. 30, iss. 6, pp. 3275–3285. ISSN 0885-8993. DOI: 10.1109/TPEL.2014.2337292.

[13] LI, W., J. FANG, H. LI and J. TANG. Position Sensorless Control Without Phase Shifter for High-Speed BLDC Motors With Low Inductance and Nonideal Back EMF. *IEEE Transactions on Power Electronics*. 2016, vol. 31, iss. 2, pp. 1354–1366. ISSN 0885-8993. DOI: 10.1109/TPEL.2015.2413593.

[14] SUNDEEP, S. and B. SINGH. Robust Position Sensorless Technique for a PMBLDC Motor. *IEEE Transactions on Power Electronics*. 2018, vol. 33, iss. 8, pp. 6936–6945. ISSN 0885-8993. DOI: 10.1109/TPEL.2017.2759761.

[15] CHEN, S., X. ZHOU, G. BAI, K. WANG and L. ZHU. Adaptive Commutation Error Compensation Strategy Based on a Flux Linkage Function for Sensorless Brushless DC Motor Drives in a Wide Speed Range. *IEEE Transactions on Power Electronics*. 2018, vol. 33, iss. 5, pp. 3752–3764. ISSN 0885-8993. DOI: 10.1109/TPEL.2017.2765355.

[16] LI, T. and J. ZHOU. High-Stability Position-Sensorless Control Method for Brushless DC Motors at Low Speed. *IEEE Transactions on Power Electronics*. 2018, Early Access. ISSN 0885-8993. DOI: 10.1109/TPEL.2018.2863735.

[17] LEE, A., C. FAN and G. CHEN. Current Integral Method for Fine Commutation Tuning of Sensorless Brushless DC Motor. *IEEE Transactions on Power Electronics*. 2017, vol. 32, iss. 12, pp. 9249–9266. ISSN 0885-8993. DOI: 10.1109/TPEL.2017.2652847.

[18] LEE, A., S. WANG and C. FAN. A Current Index Approach to Compensate Commutation Phase Error for Sensorless Brushless DC motors with Nonideal Back EMF. *IEEE Transactions on Power Electronics*. 2016, vol. 31, iss. 6, pp. 4389–4399, ISSN 0885-8993. DOI: 10.1109/TPEL.2015.2468081.

[19] LI, H., S. ZHENG and H. REN. Self-Correction of Commutation Point for High-Speed Sensorless BLDC Motor with Low Inductance and Nonideal Back EMF. *IEEE Transactions on Power Electronics*. 2017, vol. 32, iss. 1, pp. 642–651. ISSN 0885-8993. DOI: 10.1109/TPEL.2016.2524632.

[20] JIANCHENG, F., L. WENZHUO and L. HAITAO. Self-Compensation of the Commutation Angle Based on DC-Link Current for High-Speed Brushless DC Motors with Low Inductance. *IEEE Transactions on Power Electronics*. 2014, vol. 29, iss. 1, pp. 428–439. ISSN 0885-8993. DOI: 10.1109/TPEL.2013.2254499.

[21] JIANCHENG, F., Z. XINXIU and L. GANG. Precise Accelerated Torque Control for Small Inductance Brushless DC Motor. *IEEE Transactions on Power Electronics*. 2013, vol. 28, iss. 3, pp. 1400–1412. ISSN 0885-8993. DOI: 10.1109/TPEL.2012.2210251.

[22] IWASAKI, S., R. P. DEODHAR, L. YONG, A. PRIDE, Z. Q. ZHU and J. J. BREMNER. Influence of PWM on the Proximity Loss in Permanent-Magnet Brushless AC Machines. *IEEE Transactions on Industry Applications*. 2009, vol. 45, iss. 4, pp. 1359–1367. ISSN 0093-9994. DOI: 10.1109/TIA.2009.2023488.

[23] JIANCHENG, F., L. HAITAO and H. BANGCHENG. Torque Ripple Reduction in BLDC Torque Motor With Nonideal Back EMF. *IEEE Transactions on Power Electronics*. 2012, vol. 27, iss. 11, pp. 4630–4637. ISSN 0885-8993. DOI: 10.1109/TPEL.2011.2176143.

About Authors

Shahin MAHDIYOUN RAD obtained her B.Sc. in Electronics Engineering from the University of Zanjan, Iran, in 2008, and her M.Sc. in Electrical Engineering from the University of Tabriz, Iran, in 2011. She is currently working toward her Ph.D. in the Department of Electrical Engineering, Sahand University of Technology, Tabriz, Iran. Her current research interests include control of electrical drives and electrical machines.

Mohammad Reza AZIZIAN obtained his B.Sc. and M.Sc. from the University of Tabriz, Tabriz, Iran, in 1988 and 1991, respectively, and his Ph.D. from Brno University of Technology, Brno, Czech Republic, in 2003, all of which in Electrical Engineering. From 1991 to 1999, he worked as a research assistant at the Department of Electrical Engineering in Sahand University of Technology, Tabriz, Iran, where he is currently an associate professor. His research interests include sensorless control of electrical drives and the design and implementation of power converters.

Mohammad HEJRI obtained his B.Sc. degree from Tabriz University in 2000 and his M.Sc. and Ph.D. degrees from Sharif University of Technology, Tehran, Iran, in 2002 and 2010, respectively, both in electrical engineering. Since 2012, he has been an Assistant Professor with the Department of Electrical Engineering, Sahand University of Technology, Tabriz. His research interests include control theory with applications in power electronics and renewable energy.